Experimental determination of partition coefficients for rare earth and high-field-strength elements between clinopyroxene, garnet, and basaltic melt at high pressures

Article *in* Contributions to Mineralogy and Petrology · October 1998

DOI: 10.1007/s004100050437

Contrib Mineral Petrol (1998) 133: 60–68

Kevin T.M. Johnson

Experimental determination of partition coefficients for rare earth and high-field-strength elements between clinopyroxene, garnet, and basaltic melt at high pressures

Received: 1 July 1997 / Accepted: 11 May 1998

Abstract Clinopyroxene/melt and garnet/melt partition coefficients have been determined for Ti, Sr, Y, Zr, Nb, Hf, and rare earth elements from 19 doped experiments on 1921 Kilauea basalt. The experiments were carried out from 2.0 to 3.0 GPa and 1310° to 1470 °C. The purpose was to derive a set of partition coefficients for high-field-strength elements (HFSE) and rare earth elements (REE) in a systematic, linked set of experiments at P and T conditions relevant to basalt petrogenesis. These data are used in melting models to understand the development of negative HFSE anomalies observed in many abyssal peridotite clinopyroxenes. It is shown that melting can account for the observed trace element patterns in some residual peridotites, but that other processes may also be needed to account for most residual mantle compositions in mid-ocean ridge systems. It is also shown that REE are more strongly fractionated by garnet at these P-T conditions than previously thought.

Introduction

Over the years, increasingly detailed numerical models have been used to constrain melting, melt segregation, and crystallization processes in the upper mantle and crust (Gast 1969; Shaw 1970; Langmuir et al. 1977; Maaløe 1982; Johnson et al. 1990; Johnson and Dick 1992; Iwamori 1993). These models are essentially based on a mass balance of elements in melting or crystallizing systems, and rely, in large part, on precise knowledge of mineral/melt partition coefficients (D). Because clinopyroxene and garnet are the primary reservoirs of rare earth elements (REE) and high field strength elements (HFSE) in upper mantle peridotites, determination of D for these two phases is very important.

Partition coefficients are determined by measuring elemental concentrations in natural or experimentally synthesized phenocryst/matrix pairs, or by combining experiments with thermodynamic relationships and two-lattice melt models (Onuma et al. 1968; Schnetzler and Philpotts 1968, 1970; Masuda and Kushiro 1970; Banno and Matsui 1973; Shimizu and Kushiro 1975; Ray et al. 1983; Fujimaki et al. 1984; Irving and Frey 1984; Nielsen 1985; McKay et al. 1986; Nielsen 1988; Blundy and Wood 1991; Beattie 1993; Hart and Dunn, 1993; LaTourrette et al. 1993; Blundy and Wood 1994; Forsythe et al. 1994; Hack et al., 1994; Hauri et al., 1994; Nielsen et al. 1994). This paper reports results of a set of 19 experiments on natural and doped tholeiitic basalt from Kilauea run at 1310 °–1470 °C and 2.0–3.0 GPa designed to measure crystal/melt partition coefficients of Ti, Sr, Y, Zr, Nb, La, Ce, Nd, Sm, Dy, Er, Yb, Lu, and Hf in clinopyroxene and garnet. This study differs from previous partitioning studies in that the experiments were designed to produce a coherent set of partition coefficients for rare earth and high field strength elements from the same samples to eliminate uncertainties due to different conditions for each set of elements.

Experimental and analytical methods

Starting material

Starting material for the experiments was 1921 Kilauea olivine tholeiite (Tilley 1960; Yoder and Tilley 1962). The composition of the starting material is listed in Table 2. The starting material was produced by powdering and completely melting the olivine tho-

K.T.M. Johnson
Department of Geology, Bishop Museum, Honolulu, HI 96817 USA and Hawaii Center for Volcanology, University of Hawaii, Honolulu, HI 96822 USA
Tel: +1-808-848-4124, Fax: +1-808-847-8252
e-mail: kevinj@soest.hawaii.edu

Editorial responsibility: T.L. Grove

Supplementary material Table 3. Trace element concentrations (ppm) in experimental products at 2.0-3.0 GPa (abbreviations as in Table 1) has been deposited in electronic form and can be obtained from http://link.springer.de/link/service/journals/00410

leiite, then quenching to a glass. This glass was then powdered, dried at 120 °C, fused in a standard 1 atm. furnace in a Pt crucible at 1300 °C at $f_{O_2} = 10^{-8}$, quenched, and then repowdered. Variable amounts of 99.9% pure trace element oxides of Sr, Y, Zr, Nb, Hf, La, Nd, Sm, and Lu were added as spikes in different combinations to this starting powder, but total dopant was generally <1 wt% and did not exceed 2 wt% in any of the mixtures.

Experimental procedure

Experiments were done at the University of Tokyo using a half-inch solid medium piston-cylinder apparatus. Samples were loaded in graphite capsules, and then placed inside Pt capsules, heated to ~ 1000 °C to drive off volatiles, and then welded shut. These platinum capsules were loaded into 0.5 inch talc-pyrex assemblies with a graphite heater and sintered AlSiMg spacers. The assemblies were wrapped in Pb foil to minimize friction at high pressures and then loaded into the piston-cylinder apparatus. Experiments on doped and undoped charges were run from 5 to 120 h at 2.0–3.0 GPa and 1300 °–1470 °C using the piston-out technique with a −3% pressure correction (Kushiro 1976). Temperatures were measured with Pt/Pt_{90}-Rh_{10} themocouples and were controlled with a Eurotherm digital controller. No correction was made for the effect of pressure on EMF. Temperatures have a precision of ±2 °C and an accuracy of ±5 °C based on calibrations with Au and Pd. Run conditions are reported in Table 1.

Analytical methods

Samples were mounted in epoxy and polished, then analyzed with the 5-spectrometer wavelength dispersive JEOL 733 electron microprobe at University of Tokyo and by Cameca IMS-3f ion microprobe at Woods Hole Oceanographic Institution. Beam conditions for the microprobe analyses were 15 keV accelerating voltage and 10 nA beam current. A defocused beam of 10 μm was used for glass analyses and a focused 1 μm beam was used for mineral phases. Major element compositions of the phases are reported in Table 2.

Trace element compositions of the phases present in each run were determined by ion microprobe. Energy filtering was used to minimize isobaric interferences between molecular ions and the monatomic ions of interest. For Ti, Sr, Y, Zr, Nb, and Hf, a primary beam of negatively charged oxygen ions with a current of approximately 0.2 nA and a net energy of 12.55–12.65 keV was focused to a 5–8 μm-diameter spot on the sample. Positively charged secondary ions pass through an electrostatic sector and produce an energy spectrum, which is selectively sampled by using a high-energy offset of −90 eV and an energy bandpass of ±10 eV (net secondary accelerating voltage of 4400–4420 eV), and is then mass analyzed by a double-focusing mass spectrometer and counted by a 17-stage Allen type electron multiplier in pulse counting mode. For REE, a 1–2 nA primary beam was focused to a 12–20 μm spot and energy filtering of −60 eV was used. Empirical relationships between secondary ion intensities and concentrations (working curves) were used to calculate trace element concentrations. Sources of analytical uncertainty include counting error, precision and accuracy of standards analyses, calibration of mass peaks, and magnet drift. Within-run counting precision, based on averaging five replicate data blocks per analysis, is generally <1% for Ti, Sr, Y, and Zr, and doped Nb, Hf, and REE. Undoped these elements generally are measured with internal precisions of $\sim$ 5–15%. Trace element compositions of the experimental charges are reported in *CMP online Table 3*. Standard deviations about the mean are generally ±0.1–8% for glass analyses and ±3–15% for cpx, but intergrain variability in runs E8, E10, R5, and Z25-2 was ±3–25% because of larger numbers of points analyzed.

Table 1 Experimental run conditions (*gl* melt, *cpx* clinopyroxene, *gar* garnet)

Expt.[a]	T (°C)	P (GPa)	t (h)	Run Products
E4	1325	2.0	72	gl, cpx
E5	1350	2.0	30	gl, cpx
E6	1350	2.0	5	no crystals
E7	1363	2.5	16.8	gl, cpx
E8	1391	2.5	24	gl, cpx
E9	1363	2.5	120	gl, cpx
E10	1363	2.5	7	gl, cpx
E11	1391	2.5	5.3	gl, cpx
E12	1335	2.5	24	gl, cpx
R2	1325	2.0	93	gl, cpx
R3	1310	2.0	72	no crystals
R4	1340	2.7	72	gl, cpx
R5	1310	2.0	72	gl, cpx
RH1	1310	2.0	72	gl, cpx
RH2	1340	2.0	72	gl, cpx
RH30-1	1430	3.0	48	gl, cpx, gar
Z20-1	1340	2.0	48	gl, cpx
Z20-2	1325	2.0	48	gl, cpx
Z25-1	1340	2.5	47	gl, cpx
Z25-2	1390	2.5	37	gl, cpx
Z30-1	1470	3.0	48	gl, cpx

[a] "E" series – 1921 Kilauea basalt doped with ~1 wt% La, Sr, and Y. "R" series – 1921 Kilauea basalt doped with ~2000 ppm Nb, La, Nd, Sm, Lu and ~4000 ppm Hf. "RH" series – "R" doping concentrations halved by addition of more basalt, "Z" series – 1921 Kilauea basalt doped with ~2000 ppm Zr, Nb, Hf, Lu

Results

Clinopyroxene

In all runs, the melt quenched to a clear glass. Clinopyroxene was the solitary crystalline phase produced in all experiments except run RH30-1 at 1430 °C and 3.0 GPa, which also produced garnet. Glass compositions in all runs were homogeneous, and the clinopyroxene crystals were generally unzoned except in a few runs, which were not included in the calculation of partition coefficients. Because of isobaric molecular ion interferences between BaO and Eu, Eu concentrations in the liquids were not reliable and $D_{Eu}^{cpx/liq}$ is not listed for clinopyroxene. Also, Ce, Dy, Er, and Yb were not doped in the experiments so their D values are based on their natural trace abundance in the starting mixture and are less precise than the other elements. Averaged analyses are reported in Tables 2 and 3 and complete data tables are available on-line from this journal.

In order to use experimental data for partitioning studies approach to equilibrium between crystals and liquids must be demonstrated. Two methods, Fe/Mg partitioning, and zoning, were used in this study to assess approach to equilibrium in the experiments.

Based on a large number of published clinopyroxene-basalt equilibria experiments, $(Fe/Mg_{cpx})/(Fe/Mg_{glass})$ (K_D) averages 0.30 ± 0.04 at similar P, T, and composition conditions as this study. The calculated K_D of the experiments used in this study is 0.28 ± 0.01, consistent with equilibrium conditions.

Table 2 Major element concentrations (wt%) in experimental products at 2.0–3.0 GPa (abbreviations as in Table 1)[a]

Expt.	Phase	n	SiO_2	TiO_2	Al_2O_3	FeO	MnO	MgO	CaO	Na_2O	K_2O	Total
E4	gl	2	54.4(3)	2.87(9)	16.00(4)	9.6(8)	0.16(1)	5.37(1)	8.5(1.1)	2.71(2)	0.55(1)	100.2
	cpx	9	50.3(5)	1.01(12)	8.76(51)	7.50(40)	0.16(4)	13.9(3)	16.7(5)	1.12(7)	0.01(0)	99.4
E5	gl	6	50.1(4)	2.53(11)	14.2(2)	9.79(11)	0.17(7)	6.63(10)	10.4(1)	2.38(16)	0.43(4)	96.7
	cpx	10	50.9(3)	0.88(6)	7.89(23)	6.28(23)	0.15(2)	14.9(2)	17.5(2)	1.00(3)	0.02(1)	99.5
E7	gl	4	50.1(5)	2.65(9)	14.3(3)	10.5(1)	0.22(5)	5.72(13)	9.36(22)	2.61(15)	0.52(2)	95.9
	cpx	18	49.4(5)	0.84(12)	9.36(38)	6.84(22)	0.15(5)	14.2(2)	16.5(4)	1.43(12)	0.01(1)	98.7
E8	gl	4	51.6(1)	2.58(6)	14.4(1)	10.1(2)	0.16(6)	5.79(7)	10.1(1)	2.25(7)	0.46(5)	97.3
	cpx	5	51.6(3)	0.78(9)	9.68(31)	6.33(12)	0.14(2)	13.6(1)	16.0(4)	1.48(4)	0.01(1)	99.7
E9	gl	4	51.0(5)	2.96(7)	14.6(3)	10.4(3)	0.15(7)	5.10(5)	8.66(11)	2.69(13)	0.49(4)	96.0
	cpx	4	50.0(2)	0.81(1)	10.6(2)	7.76(13)	0.18(5)	13.2(2)	15.5(2)	1.77(3)	0.01(0)	99.8
E10	gl	4	51.4(5)	2.70(3)	14.5(1)	10.6(2)	0.21(3)	5.69(21)	9.03(59)	2.55(10)	0.45(6)	97.1
	cpx	6	50.6(3)	0.85(13)	9.84(32)	6.82(15)	0.17(5)	13.6(2)	15.9(4)	1.55(7)	0.01(0)	99.3
E11	gl	4	48.5(2)	2.50(5)	13.29(5)	9.67(68)	0.14(1)	6.88(10)	8.5(1.3)	2.62(10)	0.43(5)	92.5
	cpx	5	48.9(5)	0.79(5)	9.03(28)	6.15(17)	0.15(5)	14.9(2)	16.0(1.5)	1.64(5)	0.01(0)	97.7
E12	gl	3	50.8(1)	2.49(8)	14.17(3)	10.2(1)	0.15(6)	6.21(15)	10.0(3)	2.43(18)	0.41(4)	96.9
	cpx	2	50.8(5)	0.70(7)	9.01(38)	6.46(39)	0.15(1)	14.4(3)	17.2(3)	1.51(3)	0.00	100.2
R4	cpx	5	48.8(3)	1.01(7)	10.4(5)	8.21(41)	0.16(2)	13.2(5)	14.9(2)	1.81(6)	0.00	98.5
Z20-1	gl	4	51.1(2)	2.50(5)	14.0(2)	9.96(15)	0.12(6)	6.76(6)	10.5(1)	2.39(7)	0.44(3)	97.9
	cpx	10	51.3(6)	0.76(10)	7.11(95)	6.40(29)	0.15(4)	15.9(4)	16.9(4)	1.01(4)	0.02(1)	99.6
Z20-2	gl	3	50.6(1)	2.69(5)	14.6(1)	10.0(1)	0.16(5)	5.55(5)	9.68(7)	2.68(10)	0.52(1)	96.5
	cpx	12	50.7(8)	1.02(25)	7.92(56)	7.27(28)	0.20(6)	15.0(7)	16.0(5)	0.96(10)	0.02(1)	99.0
Z25-1	gl	3	52.6(5)	3.02(9)	15.3(2)	10.2(3)	0.16(3)	4.25(8)	8.65(3)	2.81(5)	0.65(3)	97.5
	cpx	12	49.5(5)	1.05(9)	10.8(5)	8.36(29)	0.21(4)	12.5(4)	15.5(3)	1.63(13)	0.01(0)	99.6
Z25-2	gl	3	51.1(4)	2.74(8)	14.5(1)	10.4(1)	0.15(4)	5.98(9)	9.77(19)	2.73(13)	0.51(3)	97.9
	cpx	17	50.8(9)	0.81(9)	9.26(39)	6.81(48)	0.16(4)	13.9(5)	16.2(4)	1.37(12)	0.01(1)	99.4
Z30-1	gl	4	52.6(3)	2.42(13)	14.1(2)	9.71(39)	0.20(7)	6.81(14)	11.0(2)	2.26(10)	0.46(4)	99.6
	cpx	4	52.2(3)	0.73(5)	10.4(2)	5.65(22)	0.12(8)	13.6(2)	16.11(5)	1.73(3)	0.02(0)	100.5
RH30-1	gl	4	51.4(3)	3.07(9)	14.4(1)	10.2(2)	0.14(7)	5.21(7)	9.24(15)	2.48(6)	0.57(4)	96.7
	cpx	3	50.2(2)	0.91(10)	11.5(2)	7.46(4)	0.20(4)	12.2(1)	15.1(2)	2.04(6)	0.02(0)	99.6
	gar	5	39.9(3)	0.82(13)	22.5(3)	13.9(3)	0.43(9)	14.2(4)	7.05(11)	0.09(3)	0.01(1)	99.0
1921 Kilauea Basalt[b]	gl		50.0	2.60	12.6	10.8	0.24	9.39	10.9	2.33	0.48	99.3

[a] Units in parentheses are one standard deviation of replicate analyses in terms of least units cited. Thus 54.4(3) should be read as 54.4 ± 0.3

[b] Tilley (1960); Yoder and Tilley (1962)

Sector zoning in cpx was observed in some runs. Because previous studies showed that [111] and [100] sectors of zoned clinopyroxenes exhibit different partitioning behavior (Shimizu 1981), the runs that produced sector zoned crystals were not used in the present partition coefficient calculations.

Partition coefficients (D) were calculated by plotting the concentrations of each element in glass and cpx and regressing a line through zero. The grand average D values are also plotted in Fig. 1 and listed in Table 4. Also plotted for comparison in Fig. 1 are partition coefficients for similar bulk compositions and experimental run conditions from two other recent studies (Hart and Dunn 1993; Hauri et al. 1994). The present results closely compare with the Hart and Dunn data and the 1.7 GPa data of Hauri et al., but are 30%–35% lower in middle and heavy rare earth elements (MREE and HREE) than the 2.5 GPa data of Hauri et al. This discrepancy may be a result of the significantly higher Ca and Al contents of cpx in the Hauri et al. 2.5 GPa run (see below in section on garnet). Also significant is the presence of a pronounced negative $D_{Zr}^{cpx/liq}$ anomaly relative to the REE, though no Hf or Ti anomalies are observed (Fig. 1).

Temperature, pressure, and composition correlations with partitioning

Experiments were conducted over a range of temperatures and pressures to evaluate temperature and pressure controls on partitioning behavior. Of the trace elements determined, only $D_{Ti}^{cpx/liq}$ showed a discernible temperature dependence (Fig. 2). This result is in accordance with other studies that have described inverse dependence of D on *T*. Blundy and Wood (1991, 1994) and Wood and Blundy (1997) expressed this relationship in thermodynamic terms, and Nielsen et al. (1994) described it in terms of structural variations related to phase compositions.

Although the major element starting composition of all the experiments was the same, the major element composition of clinopyroxene changed with pressure. In particular, Ca-Tschermak's (CaTs) molecule in cpx increased with increasing pressure as expected. Many studies have described positive correlations between Wo and CaTs contents in clinopyroxene and incompatible element partition coefficients (McKay et al. 1986; Gallahan and Nielsen 1992; Jones and McKay 1992; Forsythe et al. 1994; Hack et al. 1994; Skulski et al.

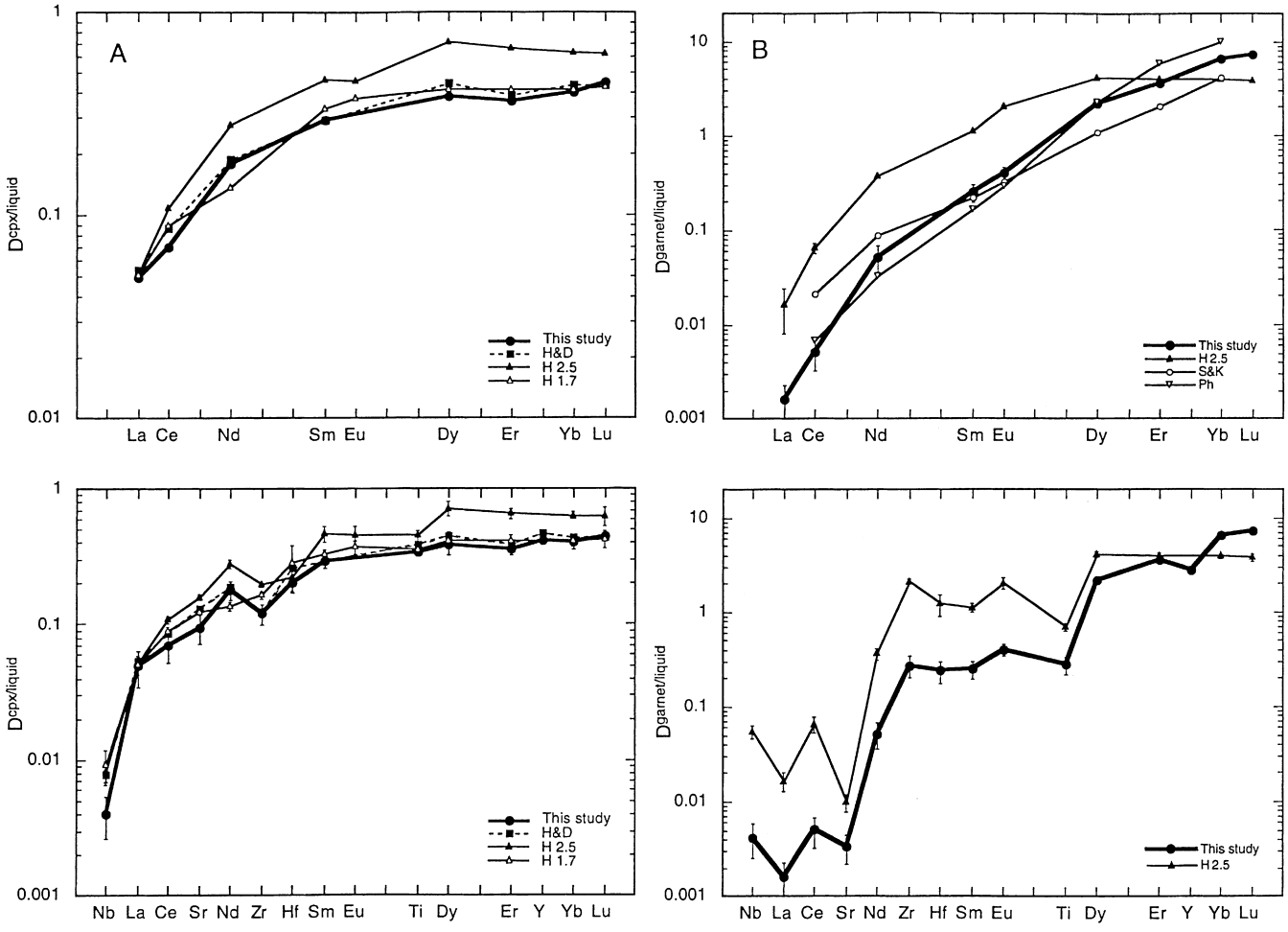

Fig. 1 **A** Cpx/melt and **B** Garnet/melt partition coefficients calculated from data in Tables 3 and 5. Also plotted for comparison are partitioning data from other authors (*Ph* Philpotts et al. 1972; *S&K* Shimizu and Kushiro 1975; *H&D* Hart and Dunn 1993; *H1.7* (1.7 GPa experiment), *H2.5* (2.5 GPa experiment) of Hauri et al. 1994). Error bars are $\pm 2\sigma$ in the cpx plot and $\pm 20\%$ in the garnet plot. See text for further discussion

1994; Gaetani and Grove 1995; Blundy et al. 1996; Wood and Blundy 1997), but the ranges in CaTs and Wo produced in those studies using a wide range of bulk compositions were much larger than the relatively limited spread of CaTs and Wo contents produced in the present study on a single bulk composition. Accordingly there was no observed correlation outside of analytical uncertainty between pressure or CaTs contents in cpx and trace element partition coefficients for the range of pressures and the elements studied.

Garnet

One large (100μ) garnet crystal and numerous small clinopyroxene crystals were grown in run RH30-1 at 3.0 GPa. Major- and trace-element concentrations of the garnet are listed in Tables 2 and 3 (clinopyroxenes were too small for ion probe analysis in this run). K_D values of 0.5 and 0.31 were calculated for the garnet and cpx, respectively, in this run.

Partition coefficients for garnet/liquid are listed in Table 4 and plotted in Fig. 1, along with patterns from Philpotts et al. (1972), Shimizu and Kushiro (1975) and Hauri et al. (1994). Partition coefficients plotted on an extended trace element diagram show positive anomalies

Table 4 $D^{cpx/liquid}$ and $D^{garnet/liquid}$ from experiments

	$D^{cpx/liquid}$	$D^{garnet/liquid}$
Ti	0.34	0.29
V		3.8
Cr		9.0
Sr	0.095	0.0025
Y	0.412	3.1
Zr	0.119	0.27
Nb	0.004	0.0031
Hf	0.200	0.24
La	0.049	0.0016
Ce	0.07	0.005
Nd	0.178	0.052
Sm	0.293	0.25
Eu		0.40
Dy	0.38	2.2
Er		3.6
Yb	0.40	6.6
Lu	0.449	7.1

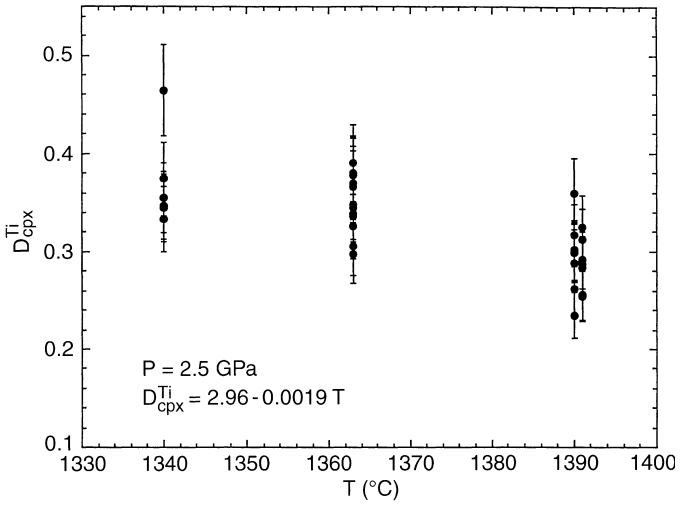

Fig. 2 Variation of D^{Ti}_{cpx} with run temperature (°C) at 2.5 GPa. Ti is the only element that showed a temperature dependence of D

in Nb and Zr and negative anomalies in Y, Ti, and Sr relative to adjacent REE (Fig. 1).

$D^{gt/liq}_{REE}$ from the present study are more fractionated (lower $D^{gt/liq}_{LREE}/D^{gt/liq}_{HREE}$) than those from the other studies. In the experiments by Shimizu and Kushiro (1975), a synthetic mixture of 30% diopside and 70% pyrope was used and element concentrations were then measured after acid dissolution of the glass from the crystals. Therefore, if some glass was not completely removed from crystals, the effect would be to increase the $D^{gt/liq}_{LREE}$ and reduce the $D^{gt/liq}_{HREE}$ producing a less fractionated partitioning pattern. Reasons for the discrepancy with the Hauri et al. (1994) data is less clear. There are subtle differences in the major element composition of the garnets from the two studies (Ca, Al, and Fe differ by 25%, 5%, and 15% respectively), but the effects of crystal composition on garnet/liquid element partitioning are not as well quantified as they are for cpx, and more work is needed in this area.

Discussion

The results of this study are in broad agreement with previously published partitioning data on cpx and garnet in rocks of similar bulk composition. However, the present work differs from others two respects: (1) a significantly larger number of data points were taken from many experiments to calculate partition coefficients, and (2) experiments were designed to determine both REE and HFSE on the same samples to address questions of HFSE anomalies in trace element patterns of many mantle rocks (Salters and Shimizu 1988; Johnson et al. 1990). $D^{cpx/liq}_{Nb}$ in cpx is lower than some published results (McCallum and Charette 1978; Dunn and McCallum 1982; Johnson and Kinzler 1989), but is in the range of others (Green et al. 1989; Hart and Dunn 1993). $D^{cpx/liq}_{REE}$ fall within published ranges (Irving 1978; McKay et al. 1986; Hart and Dunn 1993; Hack et al. 1994; Hauri et al. 1994), but show slightly greater fractionation than results at lower pressures (Grutzeck et al. 1974; Fujimaki et al. 1984).

$D^{gar/liq}_{REE}$ are more fractionated than previous results (Shimizu and Kushiro 1975). This may be a result of incomplete phase separation in the earlier study, a problem avoided by the high spatial resolution of the ion probe beam. Garnet/melt equilibrium in the present experiment can be roughly evaluated by applying diffusion coefficients for Sr and Sm in diopside (Sneeringer et al. 1984). With run conditions of 1430 °C, 3.0 GPa, and 48 h run time, a diffusion distance of over 400 microns is predicted, four times greater than the 100 micron garnet crystal being studied. Thus, chemical diffusive equilibrium is expected in the garnet.

Nd-Hf isotope systematics of MORB

Coupling of the Nd and Hf isotope systems has been used to constrain melting depths in MORB and OIB (Salters and Hart 1991). The difference between $D_{(Sm/Nd)}$ and $D_{(Lu/Hf)}$ in cpx and garnet provide the leverage in these models. The Critical Partitioning Parameter ($CPP = D_{Sm/Nd}/D_{Lu/Hf}$) Hart and Dunn 1993) is a measure of the fractionation of the parent/daughter elements for Nd and Hf isotope systems. Salters and Hart (1991) used a CPP of 1.17 in clinopyroxene and of ~ 0.2 in garnet as the basis for calling for significant degrees of melting in the garnet stability field. Hart and Dunn (1993) found $CPP^{cpx} = 0.92$. This study finds that $CPP^{cpx} = 0.73$ (range 0.52–0.92), and $CPP^{garnet} = 0.16$. This means that CPP for cpx and garnet are closer than in previous estimates making the use of this parameter less robust in distinguishing the effects of melting in the garnet stability field than previously thought. In practical terms this means that models that begin melting at depths where garnet is stable may not require as much melting in the garnet field as previously thought.

High Field strength anomalies in abyssal peridotite clinopyroxenes

In a study of trace element concentrations in clinopyroxenes from abyssal peridotites, Johnson et al. (1990) observed that Zr and Ti, when plotted with REE, showed negative concentration anomalies. Because mid-ocean ridge basalts (MORB) do not show these anomalies, Salters and Shimizu (1988) argued that abyssal peridotites and MORB were not related by any melting process. However, Johnson and Dick (1992) argued that fractional melting could produce these anomalies in peridotite cpx, but not in MORB, but their evidence was based on low pressure partitioning data from a wide variety of studies. Kelemen et al. (1990) also discussed HFSE anomalies in arc lavas and showed that they can be produced by combined mantle melting and melt-rock

reaction. The present partitioning data, produced at high pressures appropriate for melting beneath ridges and representing the entire suite of relevant elements, can be used to shed light on this problem.

Extended trace element plots of clinopyroxenes from abyssal peridotites display the HFSE anomaly (Johnson et al. 1990). One way to examine the anomalies is shown in Fig. 3, a plot of Zr/Zr* vs Ti/Ti*·Zr* and Ti* are simply the chondrite-normalized interpolated values of Zr and Ti when plotted in their relative positions with REE in incompatibility diagrams (Wood 1979; Thompson et al. 1983). Thus Zr/Zr* and Ti/Ti* are normalized concentrations of Zr and Ti relative to their interpolated values, and values less than 1 represent negative anomalies.

Figure 3 plots clinopyroxene data from abyssal peridotites as small black dots (Johnson et al. 1990; Johnson and Dick 1992) along with curves representing two melting models. The starting bulk composition in both models does not have HFSE anomalies and would plot at the crossing of the 1.0 reference lines. Melting is nonmodal perfect fractional melting with model parameters as shown in Table 5. More detailed melting models (e.g., open-system or dynamic) were not used due to the inability of even perfect fractional melting to achieve the extreme negative HFSE anomalies seen in the data. The model labeled *15% spinel* is the compositional trajectory followed by clinopyroxenes in peridotites that undergo 15% fractional melting entirely in the spinel stability field (≤2.5 GPa); the model labeled *5% garnet* and connected with dashed line to *+15% spinel* is for initial 5% melting in the garnet stability field (≥2.5 GPa) followed by an additional 15% melting in the spinel sta-

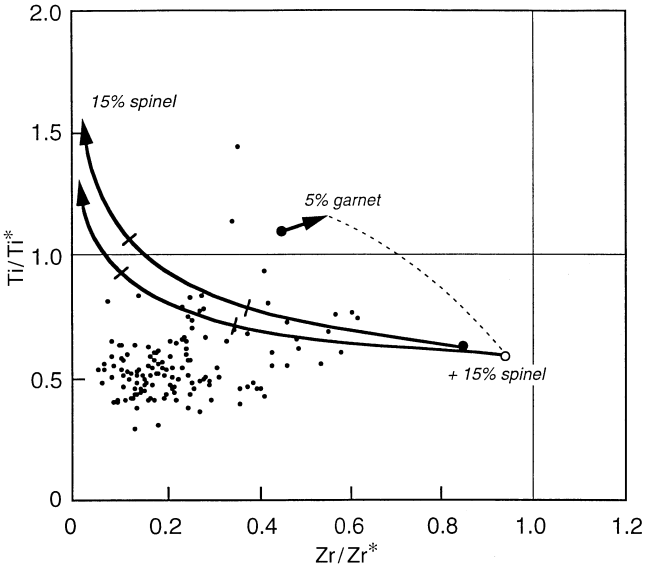

Fig. 3 Plot of Zr/Zr* vs Ti/Ti* for abyssal peridotite clinopyroxenes and melting models. Zr* and Ti* are chondrite-normalized interpolated values of Zr and Ti when plotted in their relative positions with REE in extended trace element diagrams (Wood 1979; Thompson et al. 1983). Thus Zr/Zr* and Ti/Ti* are concentrations of Zr and Ti relative to their interpolated values; values less than 1 represent negative anomalies. *Small dots* are data from Johnson et al. (1990) and Johnson and Dick (1992) and exhibit negative Zr and Ti anomalies. *Curves* are fractional melting models calculated using the parameters in Table 5 for melting in the spinel field and in the garnet field followed by the spinel field. *Hash marks* are in 5% increments. While some of the data plot close to the curves (see Fig. 4), most do not and cannot be explained by simple fractional melting alone

Table 5 Parameters used in melting models[a]

Spinel Peridotite	Mode (X)	Melt Mode (p)[b]				
Olivine	0.530	−0.060				
Opx	0.270	0.280				
Cpx	0.170	0.670				
Spinel	0.030	0.110				
Garnet Peridotite						
Olivine	0.600	0.030				
Opx	0.200	−0.160				
Cpx	0.100	0.880				
Garnet	0.100	0.090				
Element	D olivine/liq[c]	D opx/liq	**D cpx/liq**	D spinel/liq	**D garnet/liq**	C_o^d
Ce	0.00001	0.0009	**0.070**	0.0006	**0.005**	1.5
Nd	0.00007	0.009	**0.178**	0.0006	**0.052**	1.6
Zr	0.0005	0.014	**0.119**	0.070	**0.270**	1.7
Sm	0.00070	0.020	**0.293**	0.0006	**0.250**	1.8
Eu	0.00095	0.030	**0.320**	0.0006	**0.40**	1.9
Ti	0.015	0.140	**0.340**	0.150	**0.290**	2
Dy	0.004	0.060	**0.380**	0.0015	**2.200**	2
Er	0.009	0.070	**0.370**	0.003	**3.600**	2
Yb	0.023	0.100	**0.400**	0.0045	**6.600**	2

[a] Equations for calculating residual cpx compositions taken from Johnson et al. (1990)

[b] Spinel peridotite melt modes from Kinzler (1997); garnet peridotite melt modes from Walter (1997)

[c] Boldface values are data from this paper; all other D values from Kelemen et al. (1993) and references therein

[d] Approximate C1 chondrite-normalized trace element composition of MORB pyrolite based on chondritic abundances of the mantle after core formation and on isotopic and trace element composition of NMORB (Ringwood 1966; Allègre et al. 1983; Hofmann 1988; Sun and McDonough 1989); C1 chondrite normalization values of Anders and Grevesse (1989) used in the models

bility field. Melt modes in the spinel stability field are taken from Kinzler (1997) and those in the garnet stability field are taken from Walter (1998) and the phase transformation of garnet to pyroxenes and spinel is calculated as in Johnson et al. (1990). It should be noted that clinopyroxene will be exhausted in the residue of this melting scheme at about 25% total melting.

The results of this modeling demonstrate that simple melting cannot account for the HFSE anomalies observed in many of the peridotite clinopyroxenes. However, an extended trace element plot of only the peridotite cpx that fall near the model curves shows that the overall patterns are consistent with formation by 2%–7% melting in the spinel stability field (Fig. 4). However, while this model reproduces the pronounced Zr anomaly, it does not reproduce the more subtle Ti anomaly except at low degrees of melting (≤5%; curve 5S). Melting in the garnet stability field first, followed by melting in the spinel field does not produce the observed pattern shape.

Although some samples can be produced by melting alone, the majority of the data fall well below the model melting curves suggesting that either the assumptions of initial conditions are wrong or that a process other than melting alone contributes to the observed peridotite compositions. One way that the most extreme compositions can be modeled by melting alone is by invoking a starting mantle composition with extreme negative HFSE anomalies. This model is advocated by Salters and Zindler (1995) based on Zr/Sm variations in abyssal peridotites and Hf-isotope systematics in MORB. Another way that the HFSE anomalies can be increased is by increasing D_{Ti} for olivine and/or opx by an order of magnitude. Without any justification for doing this, however, it would be an arbitrary change; clearly more experiments are needed on opx and olivine REE and HFSE partitioning at high P and T conditions. We conclude that adjusting the initial conditions (starting composition, phase proportions in solid and melt, and partition coefficients) within reasonable limits cannot produce the depletions needed to reproduce the bulk of the data. Therefore, at present it appears that either a HFSE-depleted MORB source pervasively exists or a mechanism other than simple melting is needed to explain the development of the large negative HFSE anomalies observed in oceanic peridotites. Possible processes include, but are not limited to, changes in melt modes and/or D values as polybaric melting progresses (Blundy and Wood 1994; Nielsen et al. 1994; Kinzler 1997), pyroxene exsolution, or melt-rock reaction during ascent (Kelemen et al. 1990, 1993).

Conclusions

A coherent set of partition coefficients for REE and HFSE between clinopyroxene, garnet, and basaltic melt in the pressure range 2.0–3.0 GPa have been derived from a series of doped, high pressure piston cylinder experiments. The data for clinopyroxene indicate that partitioning of these elements is not a strong function of pressure or temperature, except in the case of Ti which shows a mild temperature dependence. D_{Zr} e0xhibits a subtle negative anomaly relative to adjacent REE in cpx. In garnet however, D_{Zr} exhibits a positive anomaly and D_{Ti} a negative anomaly relative to adjacent REE when plotted on an extended trace element diagram. Further, REE appear to be more strongly fractionated by garnet at the *P-T*

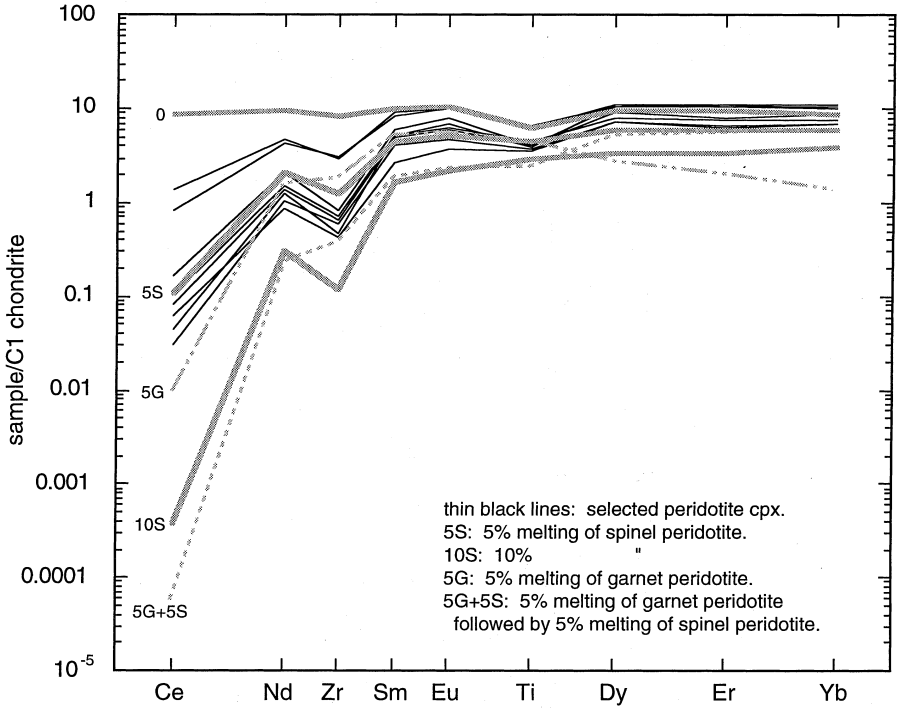

Fig. 4 Extended trace element plot of selected abyssal peridotite clinopyroxenes (*thin solid lines*) from Fig. 3 (Johnson et al. 1990; Johnson and Dick 1992) and melting models as described in the text. Model curves (*heavy gray lines*) are for perfect fractional melting of a depleted source composition (Table 5); *5S* and *10S* are 5% and 10% fractional melting in the spinel stability field; *5G* is 5% melting in the garnet stability field; *5G+5 S* is 5% melting in the garnet field followed by 5% melting in the spinel field. Melting in the spinel field alone reproduces the negative Zr anomalies, but not the negative Ti anomalies seen in the data

conditions of this study than previous experimental results indicate (Shimizu and Kushiro 1975; Hauri et al. 1994).

Application of this new set of partition coefficients to melting models based on compositions of clinopyroxenes in abyssal peridotites reveals that melting in the spinel peridotite stability pressure range can produce the HFSE anomalies in some of the data, but cannot produce the more extreme HFSE anomalies observed in many samples. Furthermore, because the ratios of $D_{Sm/Nd}/D_{Lu/Hf}$ in garnet and in clinopyroxene are closer than previously thought, claims of significant melting in the garnet peridotite stability field to produce MORB based on this parameter should be re-evaluated.

Acknowledgements The experiments in this study were conducted in the University of Tokyo laboratory of Professor Ikuo Kushiro, whose guidance and hospitality were greatly appreciated and invaluable. Technical support was provided by T. Yoshida of the University of Tokyo and Ken Burrhus of Woods Hole Oceanographic Institution. Careful reviews by V. Salters and J. Longhi improved the manuscript. This work was supported by a research fellowship from the Japan Society for the Promotion of Science.

References

Allègre CJ, Hart SR, Minster J-F (1983) Chemical structure and evolution of the mantle and continents determined by inversion of Nd and Sr isotopic data, II. Numerical experiments and discussion. Earth Planet Sci Lett 66: 191–213

Anders E, Grevesse N (1989) Abundances of the elements: meteoritic and solar. Geochim Cosmochim Acta 53: 197–214

Banno S, Matsui Y (1973) On the formulation of partition coefficients for trace elements distribution between minerals and magma. Chem Geol 11: 1–15

Beattie P (1993) The generation of uranium series disequilibria by partial melting of spinel peridotite: constraints from partitioning studies. Earth Planet Sci Lett 117: 379–391

Blundy JD, Wood BJ (1991) Crystal-chemical controls on the partitioning of Sr and Ba between plagioclase feldspar, silicate melts, and hydrothermal solutions. Geochim Cosmochim Acta 55: 193–209

Blundy JD, Wood BJ (1994) Energetics of element partitioning between minerals and melts. Mineral Mag 58A: 101–102

Blundy JD, Wood BJ, Davies A (1996) Thermodynamics of rare earth element partitioning between clinopyroxene and melt in the system CaO-MgO-Al_2O_3-SiO_2. Geochim Cosmochim Acta 60: 359–364

Dunn T, McCallum IS (1982) The partitioning of Zr and Nb between diopside and melts in the system diopside-albite-anorthite. Geochim Cosmochim Acta 46: 623–629

Forsythe LM, Nielsen RL, Fisk MR (1994) High-field-strength element partitioning between pyroxene and basaltic to dacitic magmas. Chem Geol 117: 107–125

Fujimaki H, Tatsumoto M, Aoki K (1984) Partition coefficients of Hf, Zr, and REE between phenocrysts and groundmass. Proc 14th Lunar Planet Sci Conf Part 2, J Geophys Res 89, suppl: B662–B672

Gaetani GA, Grove TL (1995) Partitioning of rare earth elements between clinopyroxene and silicate melt: crystal-chemical controls. Geochim Cosmochim Acta 59: 1951–1962

Gallahan WE, Nielsen RL (1992) The partitioning of Sc, Y, and the rare earth elements between high-Ca pyroxene and natural mafic to intermediate lavas at 1 atmosphere. Geochim Cosmochim Acta 56: 2387–2404

Gast PW (1969) Trace element fractionation and the origin of tholeiitic and alkaline magma types. Geochim Cosmochim Acta 32: 1057–1086

Green TH, Sie SH, Ryan CG, Cousens DR (1989) Proton microprobe-determined partitioning of Nb, Ta, Zr, Sr, and Y between garnet, clinopyroxene and basaltic magma at high pressure and temperature. Chem Geol 74: 201–216

Grutzeck M, Kridelbaugh S, Weill D (1974) The distribution of Sr and REE between diopside and silicate liquid. Geophys Res Lett 1: 273–275

Hack PJ, Nielsen RL, Johnston AD (1994) Experimentally determined rare-earth element and Y partitioning behavior between clinopyroxene and basaltic liquids at pressures up to 20 kbar. Chem Geol 117: 89–105

Hart SR, Dunn T (1993) Experimental cpx/melt partitioning of 24 elements. Contrib Mineral Petrol 113: 1–18

Hauri EH, Wagner TP, Grove TL (1994) Experimental and natural partitioning of Th, U, Pb and other trace elements between garnet, clinopyroxene and basaltic melts. Chem Geol 117: 149–166

Hofmann AW (1988) Chemical differentiation of the Earth: the relationship between mantle, continental crust and oceanic crust. Earth Planet Sci Lett 90: 297–314

Irving AJ (1978) A review of experimental studies of crystal/liquid trace element partitioning. Geochim Cosmochim Acta 42: 743–770

Irving AJ, Frey FA (1984) Trace element abundances in megacrysts and their host basalts: constraints on partition coefficients and megacrysts genesis. Geochim Cosmochim Acta 48: 1201–1221

Iwamori H (1993) Dynamic disequilibrium melting model with porous flow and diffusion-controlled chemical equilibration. Earth Planet Sci Lett 114: 301–313

Johnson KTM, Dick HJB (1992) Open system melting and temporal and spatial variation of peridotite and basalt at the Atlantis II Fracture Zone. J Geophys Res 97: 9219–9241

Johnson KTM, Kinzler RJ (1989) Partitioning of REE, Ti, Zr, Hf, and Nb between clinopyroxene and basaltic liquid: an ion microprobe study. Eos Trans Am Geophys Union 70: 1388

Johnson KTM, Dick HJB, Shimizu N (1990) Melting in the oceanic upper mantle: an ion microprobe study of diopsides in abyssal peridotites. J Geophys Res 95: 2661–2678

Jones JH, McKay GA (1992) REE partitioning between pyroxene/liquid and garnet/liquid: parameterization using D_{Ca}. EOS Trans Am Geophys Union 73: 607

Kelemen PB, Johnson KTM, Kinzler RJ, Irving AJ (1990) High field strength element depletions in arc basalts due to mantle-magma interaction. Nature 345: 521–524

Kelemen PB, Shimizu N, Dunn T (1993) Relative depletion of niobium in some arc magmas and the continental crust: partitioning of K, Nb, La, and Ce during melt/rock reaction in the upper mantle. Earth Planet Sci Lett 120: 111–134

Kinzler RJ (1997) Melting of mantle peridotite at pressures approaching the spinel to garnet transition: application to mid-ocean ridge basalt petrogenesis. J Geophys Res 102: 853–874

Kushiro I (1976) Changes in viscosity and structure of melt of $NaAlSi_2O_6$ composition at high pressures. J Geophys Res 81: 6347–6350

Langmuir CH, Bender JF, Bence AE, Hanson GN, Taylor SR (1977) Petrogenesis of basalts from the FAMOUS area: Mid-Atlantic Ridge. Earth Planet Sci Lett 36: 133–156

LaTourrette TZ, Kennedy AK, Wasserburg GJ (1993) Thorium-uranium fractionation by garnet: evidence for a deep source and rapid rise of oceanic basalts. Science 261: 739–742

Maaløe S (1982) Geochemical aspects of permeability controlled partial melting and fractional crystallization. Geochim Cosmochim Acta 46: 43–57

Masuda A, Kushiro I (1970) Experimental determination of partition coefficients of ten rare earth elements and barium between clinopyroxene and liquid in synthetic silicate system at 20 kilobar pressure. Contrib Mineral Petrol 26: 1209–1264

McCallum Is, Charette MP (1978) Zr and Nb partition coefficients: implications for the genesis of mare basalts, KREEP, and sea floor basalts. Geochim Cosmochim Acta 42: 859–869

McKay GA, Wagstaff J, Yang S-R (1986) Zirconium, hafnium, and rare earth element partition coefficients for ilmenite and other minerals in high-Ti lunar mare basalts: an experimental study. Proc 16th Lunar Planet Sci Conf, J Geophys Res 91: D229–D237

Nielsen RL (1985) A method for the elimination of the compositional dependence of trace element distribution coefficients. Geochim Cosmochim Acta 49: 1775–1779

Nielsen RL (1988) The calculation of combined major and trace element liquid lines of descent I. The temperature dependence of compositionally independent partition coefficients. Geochim Cosmochim Acta 52: 27–38

Nielsen RL, Forsythe LM, Hack PJ, Gallahan WE, Fisk MR, Johnston AD (1994) The compositional dependence of HFSE partitioning: a comparison between pyroxene- and magnetite-melt systematics. Mineral Mag 58A: 653–654

Onuma H, Higuchi H, Wakita H, Nagasawa H (1968) Trace element partition between two pyroxenes and the host lava. Earth Planet Sci Lett 5: 47–51

Philpotts JA, Schnetzler CC, Thomas HH (1972) Petrogenetic implications of some new geochemical data on eclogitic and ultrabasic inclusions. Geochim Cosmochim Acta 36: 1131–1166

Ray GL, Shimizu N, Hart SR (1983) An ion microprobe study of the partitioning of trace elements between clinopyroxene and liquid in the system diopside-albite-anorthite. Geochim Cosmochim Acta 47: 2131–2140

Ringwood AE (1966) The chemical composition and origin of the Earth. In: Hurley P (ed) Advances in earth science, MIT Press Cambridge, MA, pp 287–356

Salters VJM, Hart SR (1991) The mantle sources of ocean ridges, islands and arcs: the Hf-isotope connection. Earth Planet Sci Lett 104: 364–380

Salters VJM, Shimizu N (1988) World-wide occurrence of HFSE-depleted mantle. Geochim Cosmochim Acta 52: 2177–2182

Salters VJM, Zindler A (1995) Extreme $^{176}Hf/^{177}Hf$ in the sub-oceanic mantle. Earth Planet Sci Lett 129:13–30

Schnetzler CC, Philpotts JA (1968) Partition coefficients of rare-earth elements and barium between igneous matrix material and rock-forming mineral phenocrysts–I. In: Ahrens LH (ed) Origin and distribution of the elements. Pergamon, pp. 929–938

Schnetzler CC, Philpotts JA (1970) Partition coefficients of rare-earth elements between igneous matrix material and rock-forming mineral phenocrysts–II. Geochim Cosmochim Acta 34: 331–340

Shaw DM (1970) Trace element fractionation during anatexis. Geochim Cosmochim Acta 34: 237–243

Shimizu N (1981) Trace element incorporation into growing augite phenocryst. Nature 289: 575–577

Shimizu N, Kushiro I (1975) The partitioning of rare earth elements between garnet and liquid at high pressures: preliminary experiments. Geophys Res Lett 2: 413–416

Skulski T, Minarik W, Watson EB (1994) High-pressure experimental trace-element partitioning between clinopyroxene and basaltic melts. Chem Geol 117: 127–147

Sneeringer M, Hart SR, Shimizu N (1984) Strontium and samarium diffusion in diopside. Geochim Cosmochim Acta 48: 1589–1608

Sun S-S, McDonough WF (1989) Chemical and isotopic systematics of oceanic basalts: implications for mantle composition and processes. In: Saunders AD Norry MJ (eds), Magmatism in the ocean basins, Geol Soc London Spec Publ 42: 313–345

Thompson RN, Morrison MA, Dickin AP, Hendry GL (1983) Continental flood basalts....Arachnids rule OK? In: Hawkesworth CJ, Norry MJ (eds), Continental basalts and mantle xenoliths. Shiva, Nantwich, pp 158–185

Tilley CE (1960) Differentiation of Hawaiian basalts: some variants in lava suites of dated Kilauean eruptions. J Petrol 1: 47–55

Walter MJ (1998) Melting of garnet peridotite and the origin of komatiite and depleted lithosphere. J Petrol 39: 29–60

Wood BJ, Blundy JD (1997) A predictive model for rare earth element partitioning between clinopyroxene and anhydrous silicate melt. Contrib Mineral Petrol 129: 166–181

Wood DA (1979) A variably veined suboceanic upper mantle – genetic significance for mid-ocean ridge basalts from geochemical evidence. Geology 7: 499–503

Yoder HS, Tilley CE (1962) Origin of basalt magmas: an experimental study of natural and synthetic rock systems. J Petrol 3: 342–532